Astrometric Search Method for Individually Resolvable Gravitational Wave Sources with Gaia

Christopher J. Moore,[1,*] Deyan P. Mihaylov,[2] Anthony Lasenby,[3,4] and Gerard Gilmore[2]
[1]Department of Applied Mathematics and Theoretical Physics, Centre for Mathematical Sciences, University of Cambridge, Wilberforce Road, Cambridge CB3 0WA, United Kingdom
[2]Intitute of Astronomy, University of Cambridge, Madingley Road, Cambridge CB3 0HA, United Kingdom
[3]Astrophysics Group, Cavendish Laboratory, J J Thomson Avenue, Cambridge CB3 0HE, United Kingdom
[4]Kavli Institute for Cosmology, Madingley Road, Cambridge CB3 0HA, United Kingdom
(Received 16 May 2017; revised manuscript received 18 September 2017; published 29 December 2017)

Gravitational waves (GWs) cause the apparent position of distant stars to oscillate with a characteristic pattern on the sky. Astrometric measurements (e.g., those made by Gaia) provide a new way to search for GWs. The main difficulty facing such a search is the large size of the data set; Gaia observes more than one billion stars. In this Letter the problem of searching for GWs from individually resolvable supermassive black hole binaries using astrometry is addressed for the first time; it is demonstrated how the data set can be compressed by a factor of more than 10^6, with a loss of sensitivity of less than 1%. This technique was successfully used to recover artificially injected GW signals from mock Gaia data and to assess the GW sensitivity of Gaia. Throughout the Letter the complementarity of Gaia and pulsar timing searches for GWs is highlighted.

DOI: 10.1103/PhysRevLett.119.261102

Introduction.—The first detection of gravitational waves (GWs) from merging black holes has recently been achieved by LIGO [1]. LIGO can detect binaries with total masses $\lesssim 160\ M_\odot$ [2]; however, more massive supermassive black hole binaries radiate at lower frequencies, inaccessible to ground-based instruments. Observing GWs from these massive systems would shed light on the black hole mass function and the coalescence process of the host galaxies and is a target for current and future searches. The planned space-based detector LISA will detect merging binary black holes in the mass range $(10^5$–$10^7)\ M_\odot$ out to redshifts $z \lesssim 20$ [3]. Pulsar timing arrays (PTAs) use the precise timing of millisecond pulsars to search for GWs with frequencies $10^{-9} \lesssim f/\mathrm{Hz} \lesssim 10^{-7}$. Such GWs may be generated in the early inspiral of a binary in the mass range $(10^7$–$10^{10})\ M_\odot$. A GW passing over the Earth-pulsar system induces a Doppler shift which affects the pulse arrival times at Earth. By making a number of time-of-arrival measurements over a time span T PTAs achieve sensitivity to GWs with frequencies $1/T \lesssim f$ [4]. Current PTAs include NANOGrav [5], EPTA [6], PPTA [7], and the combined IPTA [8].

It is also possible to detect GWs using astrometry [9–11]. The passage of a GW over the Earth-star system changes the apparent position of the star. By making repeated astrometric measurements of many objects and recording their changing positions it is possible to turn an astrometric data set into a nHz GW observatory. The ESA mission Gaia [12] is providing an all-sky astrometric map of $> 10^9$ stars. Gaia will operate for 5–10 years, making ~80 observations (in 5 years) per source, delivering proper motion accuracy of 20 μas yr^{-1} at magnitude 15, degrading to 300 μas yr^{-1} at magnitude 20.7.

The sensitivity bandwidth of Gaia is set by the measurement timings (similar to PTAs); Gaia is sensitive to $1/T \lesssim f$. Gaia and PTAs can search for monochromatic GWs from resolvable circular binaries, stochastic backgrounds of GWs from the superposition of many binaries (or from cosmic string networks [13] or early universe perturbations [14]), or GW bursts with memory [15,16]. The astrometric analysis of a nearly monochromatic GW is considered here, for example, from a supermassive black hole binary in the early inspiral stage of its evolution.

The astrometric response to GWs.—Astrometric measurements of distant objects may be used to detect GWs; the term "star" is used to refer to any such object. It is assumed that the necessary corrections for Gaia's orbital motion have been made, and the term "Earth" is used to refer to an idealized stationary observer.

The possibility of detecting GWs via astrometry was first suggested in Ref. [9]; the astrometric deflection of a distant star was derived in Ref. [10] (also see Ref. [11]) and is summarized here. The Earth and star are assumed to be at rest in flat space. The coordinate components of the photon's four-momentum are not directly observable; instead an observer on Earth measures the *tetrad* components of the photon's four-momentum and from these is able to deduce the star's astrometric position (the unit vector $\vec{n}$), and the frequency of the starlight.

A plane monochromatic GW from the direction of the unit vector (When working with astrometry it is natural to define the sky position of the GW source, $\vec{q}$; this differs from the usual PTA convention where the GW propagation direction, $\vec{\Omega} = -\vec{q}$, is used.) $\vec{q}$ has metric perturbation $h_{\mu\nu} = \Re\{H_{\mu\nu} \exp(\mathrm{i}k_\rho x^\rho)\}$, where $H_{\mu\nu}$ are small complex

constants satisfying the usual transverse-traceless gauge conditions, and the wave vector $k^\mu = (\omega, -\omega\vec{q})$ is null. The observed photons follow null geodesics from the star to Earth; integrating the geodesic equations gives the change in the *coordinate* components of the photon four-momentum. The GW also changes the observer's tetrad: an orthonormal set of vectors parallel transported along Earth's worldline. Combining these gives the change in the tetrad components of the four-momentum, and, hence, the measured frequency and astrometric position.

The frequency perturbation is described by the redshift $1 + z \equiv \Omega_{\rm emit}/\Omega_{\rm obs}$, where

$$z = \frac{n^i n^j}{2(1 - \vec{q}\cdot\vec{n})}[h_{ij}(E) - h_{ij}(S)]; \tag{1}$$

this is the foundation of PTA efforts to detect GWs [17,18]. The redshift depends (anti)symmetrically on the metric perturbations at the "emission" and "absorption" events at the star (S) and Earth (E), respectively, (i.e., z depends only on the difference $[h_{ij}(S) - h_{ij}(E)]$). This symmetry arises from the end points of the integral along the null geodesic from the star to the Earth. The redshift can be integrated to give the timing residual signal searched for by PTAs.

The astrometric perturbation also depends on the Earth and star metric perturbations, although not symmetrically because the perturbation to the spatial vectors in the observer's tetrad depends only on the metric at Earth. The expression for the astrometric deflection is lengthy; however, it simplifies in the limit where the star is many gravitational wavelengths away from Earth [10];

$$\delta n_i = \frac{n_i - q_i}{2(1 - \vec{q}\cdot\vec{n})} h_{jk}(E) n^j n^k - \frac{1}{2} h_{ij}(E) n^j. \tag{2}$$

In this limit the astrometric deflection depends only on the "Earth term." The "star term" (or "pulsar term") is also sometimes dropped in PTA searches for individually resolvable sources because each pulsar is at a different (generally poorly constrained) distance from Earth, so the pulsar terms have different frequencies and phases and may be treated as an effective noise source. Recent searches have tended to include the pulsar terms (see, e.g., searches for individual binaries from the three PTAs [19–21], as well as Refs. [22–25]), which has the benefit of increasing the observed signal to noise at the expense of fitting for the distance to each pulsar.

Gaia's GW sensitivity comes from the large number of stars it observes. Stars are typically separated by many gravitational wavelengths; therefore, each star term will be different (as well as being suppressed by the distance to the star) whereas the Earth term is dominant and common to all stars. It is this common Earth term that Gaia aims to detect. Including the star term marginally increases the signal-to-noise ratio for the closest few stars but makes a negligible difference for the majority (e.g., a GW with wavelength $\lambda = 10^{16}$ m deflecting a typical star at $d = 10$ kpc gives a star term suppressed by $\lambda/d \approx 10^{-5}$). Figure 1 shows the Earth term astrometric deflection pattern for a field of distant stars.

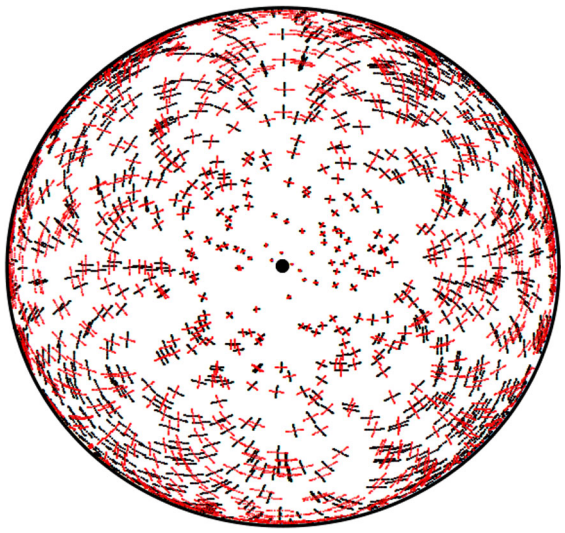

FIG. 1. Orthographic projection of the Northern hemisphere with 10^3 stars. A GW from the north pole (black dot) causes stars to oscillate at the GW frequency. The black (red) lines show movement tracks for a linearly plus (cross) polarized GW. For clarity, the GW has an unphysically large strain amplitude of $A = 0.1$. The fourfold rotational symmetry of the transverse-traceless GWs is clearly imprinted on the sky.

Data analysis.—This section describes how to search for a monochromatic GW in an astrometric data set. The likely astrophysical source of such a GW is a circular supermassive black hole binary with total mass in the range $(10^7$–$10^{10})\ M_\odot$. Such systems spend most of their lifetime in the relatively weak gravitational field where they can be safely assumed to be nonevolving over the observation period [26]. Points on the sky are denoted as $\vec{n}$, and vectors tangent to the sky are denoted as $\mathbf{h}$. For small vectors $|\mathbf{h}| \ll 1$, e.g., the GW astrometric deflection, the sum $\vec{n}' = \vec{n} + \mathbf{h}$ gives a nearby point on the sphere.

The GW metric perturbation may be written as

$$h_{ij}(\bar{\Psi}) = (A_+ H^+_{ij}(\vec{q}) e^{i\phi_+} + A_\times H^\times_{ij}(\vec{q}) e^{i\phi_\times}) e^{2\pi i f t}, \tag{3}$$

where $H^+_{ij}, H^\times_{ij}$ are the usual GW basis tensors, and $\bar{\Psi}$ is a seven-dimensional parameter vector: two amplitudes $A_+, A_\times$, two phases $\phi_+, \phi_\times$, the GW frequency f, and two angles describing the direction $\vec{q}$ to the GW source.

The data set $\mathcal{S}$ consists of N separate astrometric measurements of M stars. The different stars (and measurements) are indexed by I (and J). The observations are made at times t_J (for simplicity the t_J are assumed to be the same for all stars);

$$\mathcal{S} = \{\vec{s}_{I,J} | I = 1, 2, \ldots, M; J = 1, 2, \ldots, N\}. \tag{4}$$

Each individual measurement is a combination of the background star position $\vec{n}_I(t_J)$, instrumental noise $\mathbf{r}_{I,J}$, and (possibly) a GW;

$$\vec{s}_{I,J} = \vec{n}_I(t_J) + \mathbf{r}_{I,J} + \mathbf{h}(\bar{\Psi}; \vec{n}_I(t_J), t_J). \quad (5)$$

The background positions vary due to the star's proper motion. For each star the function $\vec{n}_I(t_J)$ is modelled as a quadratic, $\underline{\vec{n}}_I(t_J)$ and subtracted from the data;

$$\mathbf{s}_{I,J} = \vec{s}_{I,J} - \underline{\vec{n}}_I(t_J). \quad (6)$$

Thereby the background positions, proper motions, and accelerations are fit out of the data. This is the astrometric equivalent of the pulsar *timing model* and sets the low frequency sensitivity [4]. The position model can be marginalized over (see Ref. [29] in the PTA context); however, here the maximum likelihood parameters are used.

For simplicity the noise in each measurement is assumed to be identical and independent ($\sigma \equiv \sigma_{I,J}$),

$$E[\mathbf{r}_{I,J} \cdot \mathbf{r}_{I',J'}] = \sigma^2 \delta_{II'} \delta_{JJ'}. \quad (7)$$

The likelihood of $\mathcal{S}$ given the parameters $\bar{\Psi}$, assuming the star's motion has been correctly modeled and under the noise assumptions described, may be written as

$$P(\mathcal{S}|\bar{\Psi}) \propto \exp\left(\sum_{I=1}^{M}\sum_{J=1}^{N} \frac{-|\mathbf{s}_{I,J} - \mathbf{h}(\bar{\Psi}; \tilde{\mathbf{n}}_I(t_J), t_J)|^2}{2\sigma^2}\right), \quad (8)$$

where $|\cdot|$ denotes the norm of a vector on the sphere. The posterior probability follows from Bayes' theorem,

$$P(\bar{\Psi}|\mathcal{S}) = \frac{\Pi(\bar{\Psi}) P(\mathcal{S}|\bar{\Psi})}{\mathcal{Z}_s}, \quad (9)$$

with prior $\Pi(\bar{\Psi})$. Throughout this Letter uniform periodic priors for the phase angles $\phi_+, \phi_\times$, uniform in log priors for the amplitudes $A_+, A_\times$, uniform in log prior for the frequency in the range $f \sim \mathcal{U}[1/T, N/2T]$, and a uniform prior on the sphere for $\vec{q}$ are used.

The Bayesian signal evidence normalizes the distribution in Eq. (9) and is given by

$$\mathcal{Z}_{\text{signal}} = \int d\bar{\Psi}\, \Pi(\bar{\Psi}) P(\mathcal{S}|\bar{\Psi}). \quad (10)$$

The noise evidence $\mathcal{Z}_{\text{noise}}$, is simply given by the likelihood in Eq. (8) evaluated with no GW signal. The Bayes' factor $\mathcal{B} \equiv \mathcal{Z}_{\text{signal}}/\mathcal{Z}_{\text{noise}}$ is used as a detection statistic; it is assumed that any signal with $\mathcal{B} > \mathcal{B}_{\text{threshold}} = 10^{1.5}$ can be confidently detected. This is generally a conservative choice, and corresponds to Jeffrey's [30] criterion for detection with "very strong" evidence (the threshold choice is discussed in the Supplemental Material [31]); the precise detection threshold is problem specific and will depend on the details of the final Gaia data release.

The MultiNest [32] implementation of nested sampling [33] was used to sample the posterior [Eq. (9)] and evaluate the evidence [Eq. (10)].

A mock Gaia data set was constructed with $M = 10^5$ stars (approximately a factor of 10^4 less than the full Gaia catalog for computational necessity) each measured $N = 75$ times evenly spaced over a $T = 5$ year mission (the effect of nonuniform sampling is explored below). The simulated noise in each measurement was $\sigma = 100\ \mu\text{as}/\sqrt{10^4}$, reflecting an estimate of the errors in each measurement in Gaia's final data release and the reduced number of stars (the validity of this scaling and our ability to achieve the compression is established below). For each star the position model $\underline{\vec{n}}_I(t_J)$ was fitted, and subtracted according to Eq. (6).

The sensitivity is largely determined by N, M, T, and σ; the values of N, M, and T used are pessimistic estimates for the final Gaia values, while the value of σ is slightly optimistic. In particular, Gaia errors vary strongly with magnitude (see Fig. 1 of Ref. [34]); a simple estimate of the appropriate error in each measurement derived by averaging over the full magnitude range, using fits to the histogram of mean G magnitude [35], yielded a conservative estimate of 200 μas. The data set used here reflects our current best guess of Gaia's ultimate sensitivity but should be updated following future Gaia data releases.

A GW from a high mass, nonspinning binary was injected into this data set; black holes with masses $m_1 = m_2 = 5 \times 10^8\ M_\odot$ on a circular orbit of radius 1500 au at a distance of 20 Mpc (orientated with the angular momentum along the line of sight) give a circularly polarized GW with frequency $2\pi f = 2 \times 10^{-7}\ \text{s}^{-1}$ and amplitude $A_+ = A_\times = 3 \times 10^{-14}$. The GW was confidently recovered with $\mathcal{B} = 10^{4.2} > \mathcal{B}_{\text{threshold}}$ and the one-dimensional marginalized posterior distributions are shown in Fig. 2.

Compressing the Gaia data set.—Searches with $M = 10^5$ stars take days to run; the full Gaia data set with $M > 10^9$ stars is impractically large to search using the Bayesian techniques described. Here we show how the data can be greatly compressed with little loss in sensitivity. The need for compression is even greater when performing an astrometric search for a stochastic GW background because the likelihood involves the inverse of a $M \times M$ correlation matrix [11] (compression for stochastic searches will be addressed in a future publication).

A small number $\tilde{M}(\ll M)$ of points on the sky, called *virtual* stars, are selected. Each virtual star defines a Voronoi cell [36] consisting of the points nearest that virtual star. Each real star is identified with the nearest virtual star. Virtual stars are indexed by $\tilde{I} = 1, 2, \ldots, \tilde{M}$ and the Voronoi cells are denoted $\mathcal{V}_{\tilde{I}}$.

The astrometric data set is compressed into a smaller virtual data set (quantities associated with the virtual data

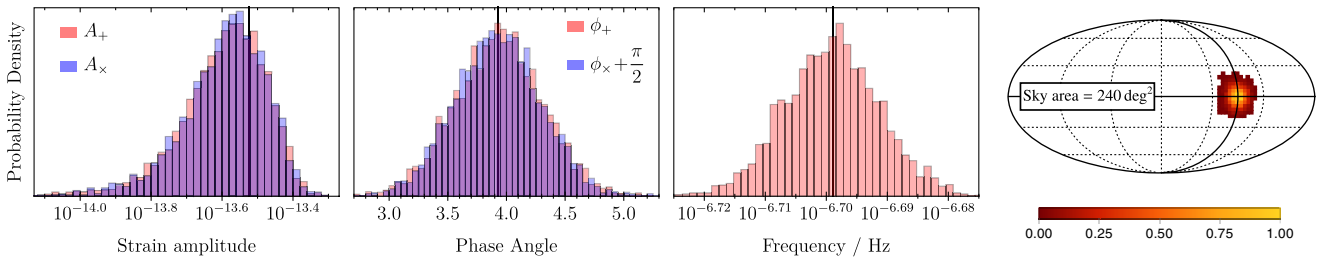

FIG. 2. One-dimensional marginalized posteriors on $\bar{\Psi}$ (black lines indicate injected values). The injected GW was circularly polarized (i.e., $\phi_+ - \phi_\times = \pi/2$) so the $\phi_\times$ posterior is shifted such that it overlaps with ϕ_+. The Mollweide sky map is shown with the area of the 68% credible region given.

are denoted with a tilde). All astrometric deflections in a set time interval for stars in a given cell are averaged;

$$\tilde{\mathbf{s}}_{\tilde{I},J} = \frac{1}{|\mathcal{V}_{\tilde{I}}|}\sum_{I\in\mathcal{V}_{\tilde{I}}}\mathbf{s}_{I,J}, \qquad \frac{1}{\tilde{\sigma}^2_{\tilde{I},J}} = \sum_{I\in\mathcal{V}_{\tilde{I}}}\frac{1}{\sigma^2_{I,J}}, \tag{11}$$

where $|\mathcal{V}_{\tilde{I}}|$ denotes the number of real stars in $\mathcal{V}_{\tilde{I}}$. The virtual data $\tilde{\mathcal{S}} = \{\tilde{\mathbf{s}}_{\tilde{I},J}|\tilde{I} = 1,\ldots,\tilde{M}; J = 1,\ldots,N\}$ [cf. Eq. (4)] may be analyzed using the techniques described above for the original data $\mathcal{S}$.

This compression would be lossless if (i) the noise was described by Eq. (7), and (ii) the astrometric deflections of all stars in a cell were parallel. The deflections vary smoothly across the sky (see Fig. 1) so as $\tilde{M}$ is increased condition (ii) becomes satisfied. In fact, for a given $\tilde{M}$ the sensitivity loss can be estimated by considering the angle between deflections of stars in the same Voronoi cell (see Fig. 3).

While condition (i) cannot be expected to hold perfectly, correlations are not expected to significantly degrade the sensitivity. Temporal correlations will be mitigated against by the fact that between measurements the spacecraft rotates into a different orientation and the starlight strikes a different part of the CCD. Spatial correlations exist, but only at the level of 3% for colocated stars, dropping to 0% for stars separated by 0.7°. As the mission proceeds correlations are expected to reduce [37]. In this first analysis we do not consider correlated errors.

The virtual star locations may be freely specified; e.g., they could be randomly generated. Here they are taken to be the midpoints of the faces of certain polyhedra. The base polyhedron was an icosahedron (the resulting Voronoi cells are called "grid 1"). Successive polyhedra were formed by constructing geodesic domes from the icosahedron—subdividing great circles between vertices into $n = 2, 3, \ldots$ smaller arcs, and constructing n^2 triangles on each face. The midpoints of the faces of the resulting polyhedra give a set of virtual stars and the resulting Voronoi cells are called "grid n." The nth grid has $\tilde{M} = 20 \times n^2$ virtual stars; grids up to $n = 10$ were used. The level of compression can be controlled by varying n.

The mock data described above were compressed onto each of the grids $n = 10, 9, \ldots, 1$ and the virtual data sets searched as before. The Bayes' factor recovered from smaller grids is reduced because stars in the larger Voronoi cells have astrometric deflections which are not parallel and partially cancel each other out in the compression [Eq. (11)]. This lower Bayes' factor reduces the maximum distance at which the source can be detected; this reduction in *horizon distance* is shown in Fig. 3. The compression loss is independent of the number of real stars. Provided grids with $n \geq 7$ are used the sensitivity loss is less than 1%. The $n = 7$ grid contains $\tilde{M} = 980$ virtual stars; therefore, the full Gaia data containing $M > 10^9$ stars can be compressed onto the $n = 7$ grid (a compression factor of $10^9/980 \approx 10^6$) with a sensitivity loss below 1%. The averaging in Eq. (11) gives these impressive compressions because of the smooth, large angle (approximately quadrupolar) pattern in Fig. 1.

Gaia's sensitivity.—Here the frequency dependence of Gaia's sensitivity is quantified, along with the effect of nonuniform time sampling (the directional sensitivity variation is quantified in the Supplemental Material [31]). Multiple mock data sets, similar to those used above, were constructed. The astrometric position of each star was measured $N = 75$ times over a $T = 5$ r period; data sets were constructed assuming both uniform time sampling

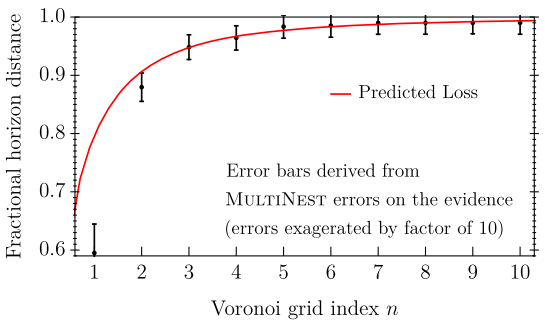

FIG. 3. The horizon distance is reduced (relative to the uncompressed data) during compression onto grid $n = 1, 2, \ldots, 10$. Shown in red is the loss estimate obtained by considering the maximum angle between deflections in the same Voronoi cell.

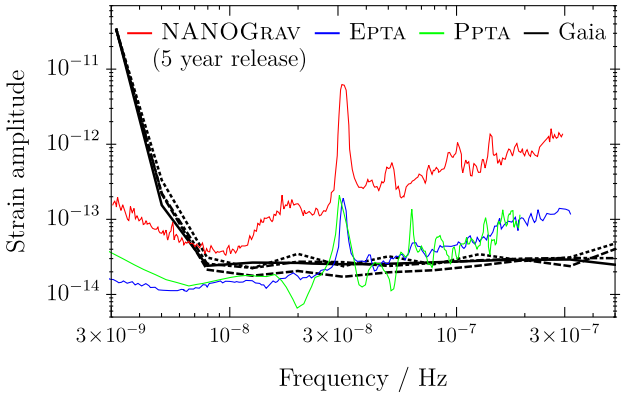

FIG. 4. The black curves show the strain sensitivity of the final Gaia data release using different time samplings (T_0, solid; T_1, dotted; T_2, dashed; T_3 dot-dashed). The colored lines show 95% PTA upper limits: NANOGrav ([19] red), EPTA ([20] blue), and PPTA ([21] green). These curves show different quantities and are only intended for approximate comparison; the NANOGrav curve is a Bayesian upper limit, the EPTA and PPTA curves are frequentist upper limits, while the Gaia curves show the amplitude necessary to achieve a (conservative) threshold Bayes' factor. It should be noted that these PTA limits are several years old and improve over time; Gaia's sensitivity will not improve further.

(T_0), and several realistic Gaia samplings, constructed using Ref. [38] (these are labeled T_1, T_2, and T_3).

Circularly polarized GWs were injected with different amplitudes and frequencies and the data compressed onto the $n = 10$ grid for analysis. For fixed frequencies in $(10^{-8.5}$–$10^{-6})$ Hz, multiple injections were used to find the minimum amplitude where the Bayes' factor exceeds $\mathcal{B}_{\text{threshold}}$ for at least 50% of noise realizations (i.e., a detection probability of $> 50\%$). The resulting sensitivity curves are shown in Fig. 4 for each T_α; the variability in the sampling has a small effect on the GW sensitivity.

The strain sensitivity of Gaia is flat above $f \gtrsim 1/T$ (where $T = 5$ yr is the mission lifetime). This is in contrast to the sensitivity of PTAs, which degrade at high frequencies. This discrepancy comes from the fact that GWs cause redshifts [Eq. (1)] and PTAs measure *timing residuals* which are the time integral of redshifts. In the frequency domain, integration over time corresponds to division by frequency; this suppresses the sensitivity of PTAs for frequencies above $f \approx 1/T$. In contrast, astrometric deflections are directly proportional to the GW strain [Eq. (2)]. This difference in slopes means that it is at mid to high frequencies, $f \gtrsim 10^{-7.5}$ Hz, where Gaia will best complement PTA efforts.

Conclusions.—GWs cause the apparent astrometric positions of stars to oscillate with a characteristic pattern on the sky [see Fig. 1 and Eq. (2)]. Gaia is the ideal observatory to make the large number of accurate astrometric measurements necessary to search for low frequency GWs using this effect. This Letter summarizes recent progress towards a practicable GW search algorithm for the fast approaching final Gaia data release. It has been shown how a large astrometric data set may be greatly compressed with little loss in sensitivity, and the GW sensitivity of Gaia to monochromatic GWs has been quantified and shown to be at a level which is potentially interesting and complementary to that from current PTA searches.

This work was supported by Grants No. MSCA-RISE-2015 690904, No. STFC ST/L000636/1, No. ST/H008586/1, No. ST/K00333X/1, and No. BIS ST/J005673/1. We thank Jonathan Gair, Stephen Taylor, Michalis Agathos, Ulrich Sperhake, and the anonymous referees for their helpful comments.

*cjm96@cam.ac.uk

[1] B. P. Abbott *et al.* (LIGO Scientific and Virgo Collaborations), Phys. Rev. Lett. **116**, 061102 (2016).
[2] B. P. Abbott *et al.* (LIGO Scientific and Virgo Collaborations), Astrophys. J. Lett. **818**, L22 (2016).
[3] P. A. Seoane *et al.* (eLISA Collaboration), arXiv:1305.5720.
[4] C J Moore, S R Taylor, and J R Gair, Classical Quantum Gravity **32**, 055004 (2015).
[5] M. A. McLaughlin, Classical Quantum Gravity **30**, 224008 (2013).
[6] M. Kramer and D. J. Champion, Classical Quantum Gravity **30**, 224009 (2013).
[7] G. Hobbs, Classical Quantum Gravity **30**, 224007 (2013).
[8] R. N. Manchester *et al.*, Classical Quantum Gravity **30**, 224010 (2013).
[9] V. B. Braginsky, N. S. Kardashev, A. G. Polnarev, and I. D. Novikov, Nuovo Cimento B **105**, 1141 (1990).
[10] T. Pyne, C. R. Gwinn, M. Birkinshaw, T. Marshall Eubanks, and D. N. Matsakis, Astrophys. J. **465**, 566 (1996).
[11] L. G. Book and É. É. Flanagan, Phys. Rev. D **83**, 024024 (2011).
[12] T. Prusti *et al.*, Astron. Astrophys. **595**, A1 (2016).
[13] A. Vilenkin, Phys. Rev. D **24**, 2082 (1981).
[14] L. P. Grishchuk, Pis'ma Zh. Eksp. Teor. Fiz. **23**, 326 (1976).
[15] J. B. Wang *et al.*, Mon. Not. R. Astron. Soc. **446**, 1657 (2015).
[16] Z. Arzoumanian *et al.*, Astrophys. J. **810**, 150 (2015).
[17] W. J. Kaufmann, Nature (London) **227**, 157 (1970).
[18] F. B. Estabrook and H. D. Wahlquist, Gen. Relativ. Gravit. **6**, 439 (1975).
[19] Z. Arzoumanian *et al.*, Astrophys. J. **794**, 141 (2014).
[20] S. Babak *et al.*, Mon. Not. R. Astron. Soc.**455**, 1665 (2016).
[21] X.-J. Zhu *et al.*, Mon. Not. R. Astron. Soc. **444**, 3709 (2014).
[22] K. J. Lee, N. Wex, M. Kramer, B. W. Stappers, C. G. Bassa, G. H. Janssen, R. Karuppusamy, and R. Smits, Mon. Not. R. Astron. Soc. **414**, 3251 (2011).
[23] C. M. F. Mingarelli, K. Grover, T. Sidery, R. J. E. Smith, and A. Vecchio, Phys. Rev. Lett. **109**, 081104 (2012).
[24] L. Boyle and U.-L. Pen, Phys. Rev. D **86**, 124028 (2012).
[25] X.-J. Zhu, L. Wen, J. Xiong, Y. Xu, Y. Wang, S. D. Mohanty, G. Hobbs, and R. N. Manchester, Mon. Not. R. Astron. Soc. **461**, 1317 (2016).

[26] For a binary to be considered monochromatic for Gaia analysis, the time scale τ, over which the GW frequency $f_{\rm GW}$ evolves, must exceed the mission lifetime of ≈10 yr. This time scale can be estimated via $\tau \approx f_{\rm GW}/\dot{f}_{\rm GW}$ using leading order post-Newtonian expressions (see, e.g., Ref. [27]). All binaries satisfy $\tau > 10$ yr up to ≈3.5 yr before merger, independent of the component masses. In contrast, these systems cannot always be considered monochromatic for PTA analysis because the pulsar terms provide snapshots of the $f_{\rm GW}$ at widely separated times allowing the frequency evolution to be measured (see, e.g., Ref. [28]).
[27] A. Buonanno, arXiv:0709.4682.
[28] S. Taylor, J. Ellis, and J. Gair, Phys. Rev. D **90**, 104028 (2014).
[29] R. van Haasteren, Y. Levin, P. McDonald, and T. Lu, Mon. Not. R. Astron. Soc. **395**, 1005 (2009).
[30] H. Jeffreys, *Theory of Probability* (Clarendon Press, New York, Oxford, 1983).
[31] See Supplemental Material at http://link.aps.org/supplemental/10.1103/PhysRevLett.119.261102 for additional calculations which assess the false alarm probability of the detection statistic and the directionality in Gaia's sensitivity to gravitational waves.
[32] F. Feroz and M. P. Hobson, Mon. Not. R. Astron. Soc. **384**, 449 (2008).
[33] J. Skilling, AIP Conf. Proc. **735**, 395 (2004).
[34] F. Mignard and S. A. Klioner, IAU Symp. **261**, 306 (2010).
[35] https://gaia.esac.esa.int/documentation/GDR1/Catalogue_consolidation/sec_cu1cva/.
[36] J.-R. Sack and J. Urrutia, in *Handbook of Computational Geometry* (North-Holland Publishing Co., Amsterdam, 2000), Chap. 5.
[37] B. Holl, L. Lindegren, and D. Hobbs, Astron. Astrophys. **543**, A15 (2012).
[38] https://gaia.esac.esa.int/gost/.